

RAEDiff: Denoising Diffusion Probabilistic Models Based Reversible Adversarial Examples Self-Generation and Self-Recovery

Fan Xing¹, Xiaoyi Zhou¹, Xuefeng Fan¹, Zhuo Tian¹, and Yan Zhao²

¹ The School of Cyberspace Security, Hainan University, Hainan, Haikou 570228, China

² Science and Technology Communication Department of Hainan Provincial Public Security Department, Hainan, Haikou, China

Abstract. Collected and annotated datasets, which are obtained through extensive efforts, are effective for training Deep Neural Network (DNN) models. However, these datasets are susceptible to be misused by unauthorized users, resulting in infringement of Intellectual Property (IP) rights owned by the dataset creators. Reversible Adversarial Examples (RAE) can help to solve the issues of IP protection for datasets. RAEs are adversarial perturbed images that can be restored to the original. As a cutting-edge approach, RAE scheme can serve the purposes of preventing unauthorized users from engaging in malicious model training, as well as ensuring the legitimate usage of authorized users. Nevertheless, in the existing work, RAEs still rely on the embedded auxiliary information for restoration, which may compromise their adversarial abilities. In this paper, a novel self-generation and self-recovery method, named as RAEDiff, is introduced for generating RAEs based on a Denoising Diffusion Probabilistic Models (DDPM). It diffuses datasets into a Biased Gaussian Distribution (BGD) and utilizes the prior knowledge of the DDPM for generating and recovering RAEs. The experimental results demonstrate that RAEDiff effectively self-generates adversarial perturbations for DNN models, including Artificial Intelligence Generated Content (AIGC) models, while also exhibiting significant self-recovery capabilities.

Keywords: Diffusion model · Reversible adversarial examples · Intellectual property protection

1 Introduction

The performance of Deep Neural Networks (DNN) [1, 13, 21, 25, 28] is heavily dependent on the quantity and quality of the training data. Artificial Intelligence Generated Content (AIGC), one of the most outstanding achievements in DNN, enabling DNN to generate content based on specific requirements and requirements, and has extensive practical applications in areas such as image

synthesis and language translation. However, as shown in Figure 1, malicious users may steal datasets for training DNN models without authorization from the dataset owners, potentially raising significant Intellectual Property (IP) concerns [2, 5, 6, 16]. As a result, a critical question needs to be considered: Can users’ images be maliciously used for DNN model training without authorization? In

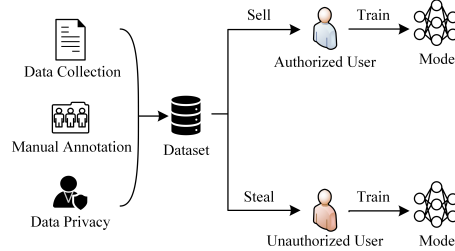


Fig. 1. Example of dataset infringement.

response to these concerns, Liu *et al.* [14] introduced the concept of Reversible Adversarial Examples (RAE). By generating adversarial examples tailored explicitly to the images, it ensures that the generation process of the adversarial examples is reversible, allowing authorized DNN models to restore the images to their original state. Applying an RAE scheme to IP protection of dataset is considered an extremely effective means for preventing malicious training on the dataset [27]. Moreover, in view of practical application scenarios, to train high-performance cloud-based models on Machine Learning as a Service (MLaaS) [22], RAEs should be compatible with Data Management Cloud Platforms (DMCP) and be able to recover and clean the datasets [27]. The existing RAE methods pose certain challenges as follows [14, 26, 27, 29, 30]:

- Challenge 1: Reversible Data Hiding (RDH) [7, 12, 33] embeds the auxiliary information into RAEs for the restoration while preserving the images’ quality, the RAE methods are predominantly leveraging RDH to achieve reversibility. However, the embedding of auxiliary information leads to the decrease of attack capability, and might make it difficult to restore.
- Challenge 2: Taking into account real-world application contexts, the current work [14, 18, 26, 27, 29, 30] lacks the capability to differentiate RAEs based on training performance due to the diverse requirements of users in DMCP.

Denosing Diffusion Probabilistic Models (DDPM) [10] is one of the widely used AIGC models for image generation. A well-trained DDPM iteratively denoises images from a randomly sampled noise through the utilization of prior knowledge to enhance the semantic representation of images [17, 19]. Inspired by the backdoor attacks on DDPM [3, 4], biasing the training process of DDPM to alternative Gaussian distributions is unlikely to significantly impact the model’s original performance.

For the purpose of overcoming Challenge 1, we designed an Adversarial Generative Process (AGP) to mislead the standard generative process of enhancing semantic representation in DDPM to generate adversarial perturbations. Since all perturbations are generated by such DDPM, it is possible to recover the perturbations without any auxiliary information through a standard generative process using a well-trained DDPM. Finally, the DDPM is biased to a Gaussian distribution controlled by the backdoor trigger, enabling the trigger to serve as a distinctive watermark within the noise introduced during AGP.

To tackle Challenge 2, **Dataset Training Performance Permission Management (DTPPM)** is introduced to provide datasets with varying training performances tailored to different requirements. An RAE-based method, named **RAEDiff**, is proposed in this study. Unlike the existing RAE methods, it enables self-generation and self-recovery of RAEs merely by a trained DDPM without any auxiliary information embedding which might impact the adversarial capability.

Our contributions are as follows:

- **RAEDiff** is introduced for the first implementation of generating RAEs through self-generation and self-recovery for IP protection of DNN image datasets. In contrast to existing RAE methods that rely on auxiliary information for restoration, **RAEDiff** attempts to unify the RAE generation and restoration by utilizing the devised AGP and leveraging the prior knowledge of the DDPM.
- The training performance requirements and the commercial value of datasets are taken into account when considering the real-world application of RAEs on DMCP. Therefore, DTPPM is proposed to provide varying training performance across multiple domains and application scenarios.
- Experiments demonstrate the feasibility of **RAEDiff** to generate RAEs for protecting DNN image datasets, which ensures the availability of the dataset for authorized users and effectively prevents unauthorized users from illegal usage.

The rest of this paper is organized as follows. The related work are reviewed in Section 2. **RAEDiff** is illustrated in Section ???. The evaluation of the proposed method is displayed in Section 3. This paper is concluded in Section 4.

2 Related work

2.1 Backdoor attack on DDPM

Research on backdoor attacks against DDPM is still in its infancy [3, 4], but it yields excellent results. The original and the backdoor attack tasks are trained under two different Gaussian distributions. A trigger is employed to shift the original task’s distribution towards that of the backdoor attack task, resulting in the model generating outputs influenced by the backdoor attacks.

2.2 Reversible Adversarial Example

Relevant experts have explored numerous different solutions to generate RAEs [14, 18, 26, 27, 29, 30] for IP protection of datasets, but they all require auxiliary information for restoration. Mao *et al.* [18] have discovered that images contain inherent structures that allow adversarial attacks to be reversed. In pursuit of reversibility in adversarial attacks, Liu *et al.* [14] first introduced the RAE method based on Reversible Data Hidding (RDH) and demonstrated its feasibility. When exploring alternative methods for generating RAEs, Yin *et al.* [30] first proposed a reversible adversarial attack based on Reversible Image Transformation (RIT) [32] and pointed out that if adversarial examples possess both attack capability and reversibility, they undoubtedly hold significant practical value. To address the passive state in dataset IP verification, Xue *et al.* [27] first proposed an active methodology for generating RAEs based on RIT. Notably, this is the sole work focusing on the generation of RAEs within the dataset. To achieve better attack capability and visual quality of RAEs, Yin *et al.* [29] proposed a method based on the independence of luminance and chrominance channels in the YUV color space. With the aim of more comprehensively examining the application of RAE in real scenarios, Xiong *et al.* [26] proposed a Perturbation Generative Network (PGN) that could generate RAEs in a black-box scenario.

In summary, there have been remarkable research achievements on RAE schemes. However, it is proved that the embedding of auxiliary information significantly impacts adversarial performances [26, 30], while existing work has not taken into account the training effectiveness of AIGC models. Therefore, aimed to generate and restore RAEs without any transformation and auxiliary information, an entirely novel approach is explored in this paper. Experiments are conducted to investigate the impact of RAEs on AIGC models.

3 Experiments

3.1 Experiment setup

Datasets, models, and implementation details We utilize two commonly used datasets: ten-class dataset CIFAR-10 (32×32) [11] and facial dataset CelebA (64×64) [15]. We followed [20, 23] and combined the three most balanced attributes of CelebA, namely Heavy Makeup, Mouth Slightly Open, and Smiling, into eight distinct classes. We adopt the diffusion models DDPM [10] and ResNet-18 [8], and follow their structures and training details. Our experiments are conducted on the basis of [3]. 50k samples on CIFAR-10 and 10k on CelebA are sampled respectively for the evaluation of performance. In order to maximize the quality of the recovered images, we trained DDPM from scratch for 500K iterations until the generated image quality approached the baseline [3]. For the provided triggers δ by authorized users, we selected Hello Kitty image, with scale factor γ set to 0.6.

Evaluation metrics Four widely-used metrics for image quality are selected for evaluation, i.e., Frechet Inception Distance(FID) [9], Learned Perceptual Image Patch Similarity(LPIPS) [31], Structure Similarity Index Measure(SSIM) [24] and Peak Signal-to-Noise Ratio(PSNR). A lower FID indicates a better reality of the image for humans, and LPIPS is employed to assess the differences between images from human perception.

3.2 Ablation Studies

The visual performance impact on RAEs of hyperparameters t_r and η are investigated, applied within **RAEDiff**, on the quality of protected dataset generation and restoration. As shown in Figure 2, when t_r is too large (*e.g.*, 40), it is challenging to recover \mathcal{D}_1^p . On the other hand, when t_r is too small (*e.g.*, 10), despite achieving better recovery quality, \mathcal{D}_1^p might lack adversarial perturbations.

When t_r is held constant, the generated \mathcal{D}_1^p remains unchanged. Figure 3 illustrates that as η increases, the time steps for restoration also increases. If η is very large (*e.g.*, 1.6), it will be over-denoising, which is most prominently observed in the reduction of PSNR. Conversely, it could result in an inability to achieve effective restoration.

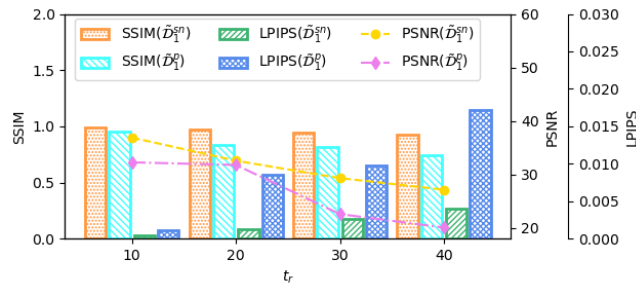


Fig. 2. Visual evaluation of $\tilde{\mathcal{D}}_1^{sn}$ and \mathcal{D}_1^p generated from different t_r when η is set to 1.4.

The selection of t_m^{sn} , t_r and η By default, the maximum time step T of DDPM is set to 1000. Therefore, we divided the interval of β_t , ranging from a minimum of 0.0001 to a maximum of 0.02, into 1000 segments using the linear approach. This allowed us to calculate the value of α_t . After calculating the $\bar{\alpha}_t = \prod_{i=1}^t \alpha_i$, we obtain $\bar{\alpha}_1 = 0.9990, \bar{\alpha}_2 = 0.9980, \bar{\alpha}_1 = 0.9960, \dots, \bar{\alpha}_T = 4.0358E-05$. According to Equation (??), it can be seen that the larger $\bar{\alpha}_t$ is, the more noise the diffusion process introduces, and the smaller the proportion of the original image becomes. For this reason, to introduce slight noise to the

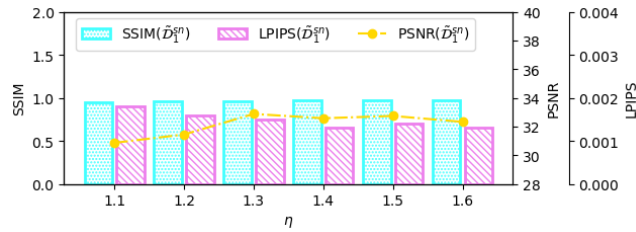


Fig. 3. Visual evaluation of $\tilde{\mathcal{D}}_1^{sn}$ generated from different η when t_r is set to 20.

dataset for grading training performance while ensuring the integrity of the data, we choose $t_m^{sn} = 1, 2$ and 3 corresponding to the permission levels 1, 2, and 3. Moreover, in order to avoid introducing additional noise and thereby increasing the difficulty of recovering the image, t_r is set to 20 and η to 1.4.

3.3 Experimental Results

In this section, the experimental results of our proposed method are presented. Additionally, we conducted an ablation study on the adverse time step t_r and reverse factor η .

Visualization results The visualization of protected datasets generation and restoration are presented in this section. As depicted in Figure 4, the protected datasets manage to maintain the quality of the original images to a significant extent while introducing adversarial noise. Additionally, the disparity between the restored images and the original images is quite small. The process of generation and restoration are shown in Figure 5.

Accuracy The dataset with permission level 1 \mathcal{D}_1^{sn} and its protected dataset \mathcal{D}_1^p along with its recovered dataset $\tilde{\mathcal{D}}_1^{sn}$ are chosen for evaluation. We followed the approach of Xue *et al.* [27], where we trained ResNet-18 from scratch. In Table 1, we presented a comparison between the training and testing accuracies of ResNet-18 trained directly on the original dataset. It can be observed that the model trained on \mathcal{D}_1^p experiences a sharp decline in performance, dropping from a testing accuracy of 94.67% to 42.75% on Cifar-10. However, $\tilde{\mathcal{D}}_1^{sn}$ can restore the original performance to a test accuracy of 94.68%. The impact on the performance of \mathcal{D}_1^p is more pronounced on CelebA, declining from a test accuracy of 81.39% to 29.40%. However, the original test accuracy can still be recovered on $\tilde{\mathcal{D}}_1^{sn}$. These demonstrate that the RAEs generated by **RAEDiff** can mislead the model training and be self-restored effectively.

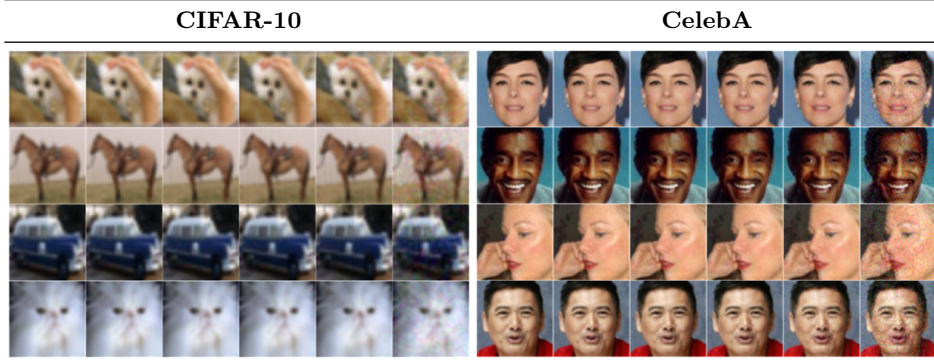


Fig. 4. Visualization of images from \mathcal{D} , \mathcal{D}_1^{sn} , \mathcal{D}_2^{sn} , \mathcal{D}_3^{sn} , $\tilde{\mathcal{D}}_1^{sn}$ and \mathcal{D}_1^p respectively on CIFAR-10 and CelebA, arranged from left to right.



Fig. 5. Visualization of the RAE generation and restoration process. The left side of each image represents the RAE generation, while the right side depicts RAE restoration.

Table 1. The training accuracy and test accuracy of the ResNet-18 model on clean, protected and recovered datasets trained on CIFAR-10 and CelebA.

		CIFAR-10		CelebA	
Method		Training Acc	Testing Acc	Training Acc	Testing Acc
Xue <i>et al.</i> [27]	Clean	96.44%	86.21%	-	-
	Protected	100.00%	38.23%	-	-
	Recovered	95.21%	85.86%	-	-
Ours	Clean \mathcal{D}_1^{sn}	97.43%	94.67%	82.86%	81.39%
	Protected \mathcal{D}_1^p	99.08%	42.75%	76.05%	29.40%
	Recovered $\tilde{\mathcal{D}}_1^{sn}$	99.12%	94.68%	81.78%	80.76%

Visual evaluation metrics We have evaluated proposed datasets \mathcal{D}_m^{sn} , \mathcal{D}_m^p , $\tilde{\mathcal{D}}_m^{sn}$ by measuring their average SSIM, PSNR, and LPIPS values in Table 2. As mentioned in Section ??, the \mathcal{D}_m^{sn} dataset is introduced slight, randomly sampled noise into the original images at different time steps diffusion process, with the purpose of distinguishing varying training performances. For the \mathcal{D}_1^{sn} , \mathcal{D}_2^{sn} , and \mathcal{D}_3^{sn} on CIFAR-10, their SSIM values are 0.997, 0.994, and 0.992, respectively. This demonstrates that the images processed through diffusion processes at different time steps can be clearly distinguished from each other. On CIFAR-10, the average SSIM value of \mathcal{D}_1^p is 0.832. It suggests that the RAEs generated by **RAEDiff** has a relatively minor impact on the original quality. In contrast, the average SSIM value of $\tilde{\mathcal{D}}_1^{sn}$ indicates a significant restoration of the original image’s structure. Furthermore, the LPIPS values for both \mathcal{D}_1^p and $\tilde{\mathcal{D}}_1^{sn}$ are within an extremely small numerical range (0.0086 and 0.0013, respectively). Consequently, this signifies that both \mathcal{D}_1^p and $\tilde{\mathcal{D}}_1^{sn}$ possess differences from the original images that are hardly perceptible to the human. For \mathcal{D}_1^p , the changes in SSIM, PSNR, and LPIPS in CIFAR-10 are smaller compared to CelebA. We attribute this to the fact that CelebA images are larger and more complex than CIFAR-10. Nonetheless, **RAEDiff** has demonstrated its strong reversibility, as evidenced by the high SSIM on $\tilde{\mathcal{D}}_1^{sn}$.

Table 2. The average SSIM, PSNR and LPIPS of \mathcal{D}_1^{sn} , \mathcal{D}_2^{sn} , \mathcal{D}_3^{sn} , \mathcal{D}_1^p , $\tilde{\mathcal{D}}_1^{sn}$ and $\tilde{\mathcal{D}}_1^{atk}$ on CIFAR-10 and CelebA.

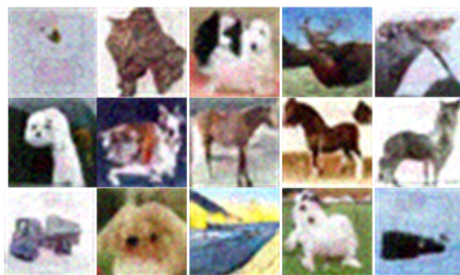
	Metrics	\mathcal{D}_1^{sn}	\mathcal{D}_2^{sn}	\mathcal{D}_3^{sn}	\mathcal{D}_1^p	$\tilde{\mathcal{D}}_1^{sn}$	$\tilde{\mathcal{D}}_1^{atk}$
CIFAR-10	SSIM	0.997	0.994	0.992	0.832	0.969	0.787
	PSNR	48.90	45.73	43.68	31.79	32.58	27.96
	LPIPS	1.288E-05	4.515E-05	7.067E-05	0.0086	0.0013	0.0121
CelebA	SSIM	0.990	0.983	0.977	0.689	0.945	-
	PSNR	48.73	45.54	43.48	24.20	34.70	-
	LPIPS	0.0001	0.0002	0.0003	0.0322	0.0036	-

Frechet Inception Distance The FID performance of fine-tuned model on the research of Chen *et al.* [3] is treated as the baseline for evaluation. In addition, we conducted training for the DDPM model while assessing the FID of images generated from noise, following a methodology akin to their prior research. The corresponding FID results for our experiments, encompassing both the protected dataset \mathcal{D}_1^p and the recovered dataset \mathcal{D}_1^{sn} at the proposed permission level 1, have been summarized in Table 3. The observation of a significant impact on the FID of the protected dataset \mathcal{D}_1^p indicates that AIGC models are difficult to train on these unrealistic datasets. Nevertheless, despite this influence, the recovered dataset $\tilde{\mathcal{D}}_1^{sn}$ retains the original performance to a great extent.

Table 3. The FID of generated images from noise along with \mathcal{D}_1^{sn} , \mathcal{D}_1^p and $\tilde{\mathcal{D}}_1^{sn}$ on CIFAR-10 and CelebA.

Method		CIFAR-10 CelebA	
Chen <i>et al.</i> [3]	From noise	4.74	5.44
Ours	From noise	4.59	5.60
	Clean \mathcal{D}_1^{sn}	0.33	0.69
	Protected \mathcal{D}_1^p	85.48	62.63
	Recovered $\tilde{\mathcal{D}}_1^{sn}$	1.00	3.92

Robustness RAEDiff effectively maintains its confidentiality. However, we also need to consider the possibility of attacks, where attackers have a comprehensive understanding of our protection mechanisms attempting to restore the images. To address this concern, we conducted a simulation experiment. We assumed that attackers had managed to steal the protected dataset \mathcal{D}_1^p from authorized users. Moreover, they possess hardware and software conditions similar to ours. With these resources, attackers trained an equivalent DDPM using \mathcal{D}_1^p . The only difference is that their model does not introduce any bias to the Gaussian distribution but instead uses the original standard Gaussian distribution. After illegal training, they get $\tilde{\mathcal{D}}_1^{atk}$, the performance of $\tilde{\mathcal{D}}_1^{atk}$ is shown in the last column of Table 2. It can be observed that due to the profound impact of the protected dataset on the AIGC model, even if an attacker were to train a DDPM using the same approach as ours, they would be unable to restore the original images. Instead, this would lead to further degradation in image quality. Meanwhile, the generated images from noises on attackers’ DDPM are shown in Figure 6, demonstrating that our protected dataset similarly exerts a significant influence on the AIGC model. Hence, even when equipped with knowledge about our method, attackers are unable to effectively recover the images.

**Fig. 6.** Visualization of images generated from attacker’s DDPM. The DDPM trained on the protected dataset has met a significant performance degradation. Additionally, it is able to discern the trigger in the generated images.

Theoretical reversibility We exclusively trained the DDPM on a subset of 50 CIFAR-10 images to explore the theoretical reversibility achievable under ideal conditions using our proposed method. As shown in Figure 8, **RAEDiff** could be used solely through the DDPM’s prior knowledge of the data to recover \mathcal{D}_1^p to $\tilde{\mathcal{D}}_1^{sn}$, achieving great self-recovery after fully fitting the data.

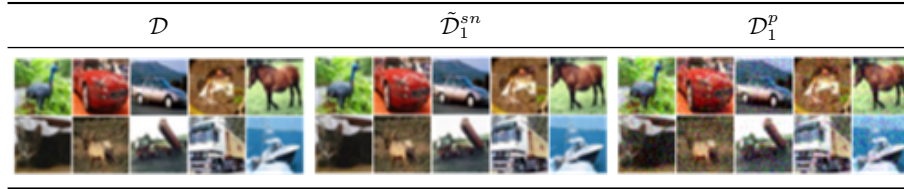


Fig. 7. Visualization of \mathcal{D} , $\tilde{\mathcal{D}}_1^{sn}$ and \mathcal{D}_1^p on CIFAR-10 under ideal conditions. The SSIM, PSNR, and LPIPS values for $\tilde{\mathcal{D}}_1^{sn}$ are 0.995, 36.68, and 0.0003, respectively.

4 Conclusion

In this paper, a self-generation and self-recovery RAE method based on DDPM with a biased Gaussian distribution is proposed. Experiments are conducted to examine the impact of RAEs on the training performance of the AIGC model for the first time. Compared to existing RAE methods, our proposed method has a significant impact on model testing accuracy, resulting in a substantial increase (e.g., 42.75% testing accuracy on CIFAR-10). Furthermore, it first effectively restores RAEs to the original image without any auxiliary information (e.g., SSIM of 0.969 on CIFAR-10). The model accuracy and visual evaluation metrics results demonstrate that our proposed method effectively introduces adversarial perturbations to both the classification model and the AIGC model. In future research, we intend to optimize the AGP in the diffusion model and explore the possibility of achieving constraints through loss functions to enhance the adversarial attack strength of RAEs. Furthermore, we aim to examine the impact of various network structures on the diffusion model to enhance its ability to refine the introduced noise on RAEs for superior visual quality.

References

1. Banesh, D., Petersen, M.R., Ahrens, J., Turton, T.L., Samsel, F., Schoonover, J., Hamann, B.: An image-based framework for ocean feature detection and analysis. *Journal of Geovisualization and Spatial Analysis* **5**, 1–21 (2021)
2. Chen, C., Wu, Z., Lai, Y., Ou, W., Liao, T., Zheng, Z.: Challenges and remedies to privacy and security in aigc: Exploring the potential of privacy computing, blockchain, and beyond. *arXiv preprint arXiv:2306.00419* (2023)

3. Chen, W., Song, D., Li, B.: Trojdiff: Trojan attacks on diffusion models with diverse targets. In: Proceedings of the IEEE/CVF Conference on Computer Vision and Pattern Recognition. pp. 4035–4044 (2023)
4. Chou, S.Y., Chen, P.Y., Ho, T.Y.: How to backdoor diffusion models? In: Proceedings of the IEEE/CVF Conference on Computer Vision and Pattern Recognition. pp. 4015–4024 (2023)
5. Dai, L., Mao, J., Xu, L., Fan, X., Zhou, X.: Balancing robustness and covertness in nlp model watermarking: A multi-task learning approach. In: 2023 IEEE Symposium on Computers and Communications (ISCC). pp. 1376–1382. IEEE (2023)
6. Fan, X., Zhou, X., Zhu, B., Dong, J., Niu, J., Wang, H.: Survey of copyright protection schemes based on dnn model. Journal of Computer Research and Development **59**(2022-05-953), 953–977 (2022)
7. Fu, D., Zhou, X., Xu, L., Hou, K., Chen, X.: Robust reversible watermarking by fractional order zernike moments and pseudo-zernike moments. IEEE Transactions on Circuits and Systems for Video Technology (2023)
8. He, K., Zhang, X., Ren, S., Sun, J.: Deep residual learning for image recognition. In: Proceedings of the IEEE conference on computer vision and pattern recognition. pp. 770–778 (2016)
9. Heusel, M., Ramsauer, H., Unterthiner, T., Nessler, B., Hochreiter, S.: Gans trained by a two time-scale update rule converge to a local nash equilibrium. Advances in neural information processing systems **30** (2017)
10. Ho, J., Jain, A., Abbeel, P.: Denoising diffusion probabilistic models. Advances in neural information processing systems **33**, 6840–6851 (2020)
11. Krizhevsky, A., Hinton, G., et al.: Learning multiple layers of features from tiny images (2009)
12. Kumar, S., Gupta, A., Walia, G.S.: Reversible data hiding: A contemporary survey of state-of-the-art, opportunities and challenges. Applied Intelligence pp. 1–34 (2022)
13. Li, P., Tu, S., Xu, L.: Deep rival penalized competitive learning for low-resolution face recognition. Neural Networks **148**, 183–193 (2022)
14. Liu, J., Zhang, W., Fukuchi, K., Akimoto, Y., Sakuma, J.: Unauthorized ai cannot recognize me: Reversible adversarial example. Pattern Recognition **134**, 109048 (2023)
15. Liu, Z., Luo, P., Wang, X., Tang, X.: Deep learning face attributes in the wild. In: Proceedings of the IEEE international conference on computer vision. pp. 3730–3738 (2015)
16. Long, D., Jing, Z., Xuefeng, F., Xiaoyi, Z.: Nlp neural network copyright protection based on black box watermark. Chinese Journal of Network & Information Security **9**(1) (2023)
17. Lugmayr, A., Danelljan, M., Romero, A., Yu, F., Timofte, R., Van Gool, L.: Repaint: Inpainting using denoising diffusion probabilistic models. In: Proceedings of the IEEE/CVF Conference on Computer Vision and Pattern Recognition. pp. 11461–11471 (2022)
18. Mao, C., Chiquier, M., Wang, H., Yang, J., Vondrick, C.: Adversarial attacks are reversible with natural supervision. In: Proceedings of the IEEE/CVF International Conference on Computer Vision. pp. 661–671 (2021)
19. Nair, N.G., Mei, K., Patel, V.M.: At-ddpm: Restoring faces degraded by atmospheric turbulence using denoising diffusion probabilistic models. In: Proceedings of the IEEE/CVF Winter Conference on Applications of Computer Vision. pp. 3434–3443 (2023)

20. Nguyen, A., Tran, A.: Wanet–imperceptible warping-based backdoor attack. arXiv preprint arXiv:2102.10369 (2021)
21. Ning, X., Tian, W., Yu, Z., Li, W., Bai, X., Wang, Y.: Hcfnn: high-order coverage function neural network for image classification. *Pattern Recognition* **131**, 108873 (2022)
22. Ribeiro, M., Grolinger, K., Capretz, M.A.: Mlaas: Machine learning as a service. In: 2015 IEEE 14th international conference on machine learning and applications (ICMLA). pp. 896–902. IEEE (2015)
23. Salem, A., Wen, R., Backes, M., Ma, S., Zhang, Y.: Dynamic backdoor attacks against machine learning models. In: 2022 IEEE 7th European Symposium on Security and Privacy (EuroS&P). pp. 703–718. IEEE (2022)
24. Wang, Z., Bovik, A.C., Sheikh, H.R., Simoncelli, E.P.: Image quality assessment: from error visibility to structural similarity. *IEEE transactions on image processing* **13**(4), 600–612 (2004)
25. Wei, T., Chen, D., Zhou, W., Liao, J., Tan, Z., Yuan, L., Zhang, W., Yu, N.: Hairclip: Design your hair by text and reference image. In: Proceedings of the IEEE/CVF Conference on Computer Vision and Pattern Recognition. pp. 18072–18081 (2022)
26. Xiong, L., Wu, Y., Yu, P., Zheng, Y.: A black-box reversible adversarial example for authorizable recognition to shared images. *Pattern Recognition* **140**, 109549 (2023)
27. Xue, M., Wu, Y., Zhang, Y., Wang, J., Liu, W.: Dataset authorization control: protect the intellectual property of dataset via reversible feature space adversarial examples. *Applied Intelligence* **53**(6), 7298–7309 (2023)
28. Yang, J., Li, C., Zhang, P., Xiao, B., Liu, C., Yuan, L., Gao, J.: Unified contrastive learning in image-text-label space. In: Proceedings of the IEEE/CVF Conference on Computer Vision and Pattern Recognition. pp. 19163–19173 (2022)
29. Yin, Z., Chen, L., Lyu, W., Luo, B.: Reversible attack based on adversarial perturbation and reversible data hiding in yuv colorspace. *Pattern Recognition Letters* **166**, 1–7 (2023)
30. Yin, Z., Wang, H., Chen, L., Wang, J., Zhang, W.: Reversible adversarial attack based on reversible image transformation. arXiv preprint arXiv:1911.02360 (2019)
31. Zhang, R., Isola, P., Efros, A.A., Shechtman, E., Wang, O.: The unreasonable effectiveness of deep features as a perceptual metric. In: Proceedings of the IEEE conference on computer vision and pattern recognition. pp. 586–595 (2018)
32. Zhang, W., Wang, H., Hou, D., Yu, N.: Reversible data hiding in encrypted images by reversible image transformation. *IEEE Transactions on multimedia* **18**(8), 1469–1479 (2016)
33. Zhou, X., Hou, K., Zhuang, Y., Yin, Z., Han, W.: General pairwise modification framework for reversible data hiding in jpeg images. *IEEE Transactions on Circuits and Systems for Video Technology* (2023)